Text S1. PTR-MS calibration

The standard gases used in PTR-MS calibration include formaldehyde (MW 30.03), methanol (MW 32.04), acetonitrile (MW 41.05), acetaldehyde (MW 44.05), acetone (MW 58.08), dimethyl sulfide (MW 62.13), isoprene (MW 68.12), methacrolein (MW 70.09), 2-butanone (MW 72.11), benzene (MW 78.11), toluene (MW 92.14), 3-hexenol (MW 100.16), o-xylene (MW 106.16), chlorlbenzene (MW 112.01), 1,2,4-trimethylbenzene (MW 120.19), naphthalene (MW 128.18), and 1,2-dichlorobenzene (MW 147.00). The zero air and diluted standard gas (with 10 ppbv) are measured for several cycles, respectively. Based on the PTR-MS Viewer 3 software, the transmission features of the above masses are calculated, thereby a transmission curve can be made. Accordingly, the transmission values of the species which are not mentioned above can be estimated to calculate the concentrations (Taipale et al., 2008).

Text S2. PMF analysis results of OA from ACSM

Positive matrix factorization (PMF) analysis is performed for 2 factors in order to figure out the secondary component in OA, and the solution with Fpeak=0 is chosen as the optimal results. Finally, the total OA in Beijing was resolved into a hydrocarbon-like OA (HOA) factor and oxygenated OA (OOA) factor, and the relevant mass spectra, time series, diurnal variations, proportion, and correlations with external tracers of the OA factors are displayed in Fig. S1 and S2.

Text S3. Input VOC data for PMF model

According to the user's guide, PMF is a multivariate factor analysis tool that decomposes a matrix of speciated sample data into two matrices: factor contributions (G) and factor profiles (F). As a receptor model, the goal of this model is to solve the chemical mass balance (CMB) between measured species concentrations and source profiles, and the equation can be shown as follows:

$$x_{ij} = \sum_{k=1}^{p} g_{i,k} f_{k,i} + e_{i,j} \qquad (S1)$$

Where matrix X represent the ambient data with i number of samples and j species. In brief, $g_{i,k}$ stands for the contribution of kth factor in the ith sample, while $f_{k,j}$ is the

concentration of j_{th} compound in the k_{th} source, with the relevant residual e_{ij}.

PMF uses sample concentration and the corresponding uncertainty ($u_{i,j}$) provided by the user to weight individual data. The function of parameter Q mentioned in the manuscript is:

$$Q = \sum_{i=1}^{n}\sum_{j=1}^{m}\left[\frac{x_{ij} - \sum_{k=1}^{p} g_{ik}f_{kj}}{u_{ij}}\right]^2 \quad (S2)$$

Q (robust) is more generally used to define the optimal solutions, which is calculated with the points whose uncertainty-scaled residual is not greater than 4. In addition, Q_{exp} is also an important parameter which equals to (number of non-weak data values in X) - (numbers of elements in G and F). Q/Q_{exp} graphs are generally used to examine if the database is well modeled (Sarkar et al., 2017; Zheng et al., 2018).

In this study, species with high signal-to-noise ratio (S/N) are put into the concentration data file (VOC species is listed in Table S1). Besides, an equation-based uncertainty file is prepared, in which MDL is defined as 3σ baseline noise and the error fractions (EF) are estimated according to the observed data. When the sample concentration is larger than the corresponding MDL, uncertainty ($u_{i,j}$) is calculated as:

$$u_{i,j} = \sqrt{(EF \times Concentration)^2 + (MDL)^2} \quad (S3)$$

As the concentration is less than or equal to the MDL, $u_{i,j}$ is calculated as:

$$u_{i,j} = \frac{5}{6} \times MDL \quad (S4)$$

Text S4. Calculation of PSCF and CWT

In this study, the domain area is divided into i×j grid cells, and the PSCF can be defined as:

$$PSCF_{ij} = \frac{n_{ij}}{m_{ij}} \quad (S5)$$

Where m_{ij} represents the number of trajectory endpoints that fell in the *i j*th cell, and n_{ij} represent the number of endpoints that exceeded the criterion (the 75th percentile of the targeted source concentration in this study) in the same cell. When n_{ij} is lower than 3 times of the average number of trajectory endpoint on each grid (n_{ave}), a weighted

potential source contribution function (WPSCF; W(n_{ij})) should be multiplied to the PSCF value. W(n_{ij}) can be expressed as:

$$W(n_{ij}) = \begin{cases} 1, & n_{ij} > 3n_{ave} \\ 0.7, & 3n_{ave} > n_{ij} > 1.5n_{ave} \\ 0.42, & 1.5n_{ave} > n_{ij} > n_{ave} \\ 0.05, & n_{ave} > n_{ij} \end{cases} \quad (S6)$$

The CWT is defined as:

$$C_{ij} = \frac{\sum_{l=1}^{M} C_l \cdot \tau_{ijl}}{\sum_{l=1\mathrm{q}}^{M} \tau_{ijl}} \quad (S7)$$

where C_{ij} represents the average weight concentrations in the *i j*th cell, and C_l is the targeted source concentration observed when trajectory *l* observed. Besides, τ_{ijl} is the number of trajectory endpoints in the *i j*th cell associated with the C_l. The weighting function (S6) was also used in the CWT analyses.

Text S5. Diurnal variation of meteorological parameters and inorganic pollutants

In Fig. S3, the lowest point of temperature occurs around 7:00 LT, and low-level temperature inversion is prone to emerge after sunrise. Therefore, wind speed is low and the air pressure reaches to the peak around 9:00 LT, which would lead to an accumulation of pollutants. The wind speed increases as the temperature rises in daytime. Combined with the characteristics of air pressure, the best atmospheric diffusion appears around 16:00 LT.

According to Fig. S4, the tracer of vehicle exhaust, NO_X, shows bimodal-like features. The 8:00 LT peak is evidently related to traffic rush hour, and the concentration rebounds after 18:00 LT. Because the freight trucks are not allowed to enter into the urban zone in daytime, their emissions in nighttime might be higher, contributing to the high level from 22:00 LT to 2:00 LT in next day. Unlike most studies, the concentration of SO_2 is highest at noon, which might own to the advection transport from the more intense source, similar to the cases in Shijiazhuang (Hebei, China) and Bhubaneswar (India) (Ge et al., 2018; Mallik et al., 2019). Fig. S5 shows the relationship among wind direction, wind speed, and SO_2 concentration, which could verify the above conjecture. The daily change character of CO is bimodal as well, but

the variation ratio is moderate, indicating the significance contribution from other combustion sources except for vehicle exhaust.

Text S6. Source identification

Fig. S6 (a and b) shows the variation tendency of the parameter Q/Q_{exp} ratio with the factor number increases. Accordingly, the ratio declines due to additional factors, and the low decrement appears when the factor number change from 5 to 7. Combined with the factor profile characteristics, 6 factors are defined, and the Q/Q_{exp} ratio is 1.19. Profiles of the resolved sources have clear distinction according to Fig. S7. Factor 1 has high contribution to the biogenic VOCs including isoprene (m/z 69) and terpenes (m/z 137). Besides, this factor contains certain amounts of isocyanic acid (m/z 44), as well as some OVOCs including MACR+MVK (m/z 71), phenol (m/z 95), cresols (m/z 109), and dimethylphenols (m/z 123) et al., which are secondary products from photochemical reactions (Roberts et al., 2014; Zhang et al., 2017; Coeur-Tourneur et al., 2006). Generally, biogenic emissions and atmospheric chemical process are closely related to temperature and sunlight, and the diurnal characteristics in Fig. S8 coincide with this rule. It should be pointed out that m/z 107 and 121 are mixed in this factor, one of the reason is that benzaldehyde has the similar molecular weight as C8 aromatics, and another reason is that the solvent evaporation is temperature dependent thereby C8 and C9 aromatics are difficult to completely isolated using the current linear model.

Factor 2 is identified as solvent evaporation source characterized by significant loading of benzene (m/z 79), toluene (m/z 93), styrene (m/z 105), C8 aromatics (m/z 107), C9 aromatics (m/z 121), and C10 aromatics (m/z 135). As many previous studies show, the aromatics are major VOCs emitted from paint applications (Yuan et al., 2010; Yang et al., 2018; Li et al., 2019), and this is consistent with the real situation in Xinxiang according to the Multi-resolution Emission Inventory for China (http://www.meicmodel.org, last access: 15 November, 2018). In Hongqi district, there are a lot of buildings under construction and many equipment manufacturing plants involving coating process, resulting in the usage of construction and industrial solvents. In the daily variation diagram, contribution peaks around 14:00 LT is attributable to

temperature elevation, while the peaks around 2:00 LT might own to the night construction and transport activities (such as loading wastes and unloading raw materials).

Acetonitrile (m/z 42) is typical tracer of biomass burning, and ethanol (m/z 47), and butyric acid (m/z 89) usually exist in combustion process (Yuan et al., 2010; Zhou et al., 2019). Combined with the diurnal variation in Fig. S8 the third factor is mostly influenced by residential heating by consuming solid fuels including biomass and coal. During night, with the increasing demand of heating, the contribution of this factor is rising, reaching to the high level after 22:00 LT. The peak appears at 8:00 LT might be influenced by both inversion layer and residential activities such as making fire in suburban.

Factor 4, 5 and 6 contains high proportion of inorganic tracers. Based on the MEIC model, SO_2, NOx, and CO in Xinxiang are majorly emitted from thermal power generation, motor vehicles, and industrial process, respectively. Besides, the benzene/toluene (B/T) ratio can also be referred when identifying source types. The B/T ratio of factor 4 is about 1.19, within the observed range in the investigations of power plants in China (Yan et al., 2016). And the daily variation diagram shows that the contribution of this source is relatively high in daytime, resulting from the emission regular and transport contribution (like SO_2). The B/T ratio of factor 5 is 0.84 in this study, which is not far from the empirical value (0.6) for vehicle exhaust (Barletta et al., 2005). Besides, bimodality in diurnal variation could further verify the vehicle exhaust source. The B/T ratio of the last factor is 2.05, reflecting the high usage of benzene, and the contribution is stable during day according to Fig. S8.

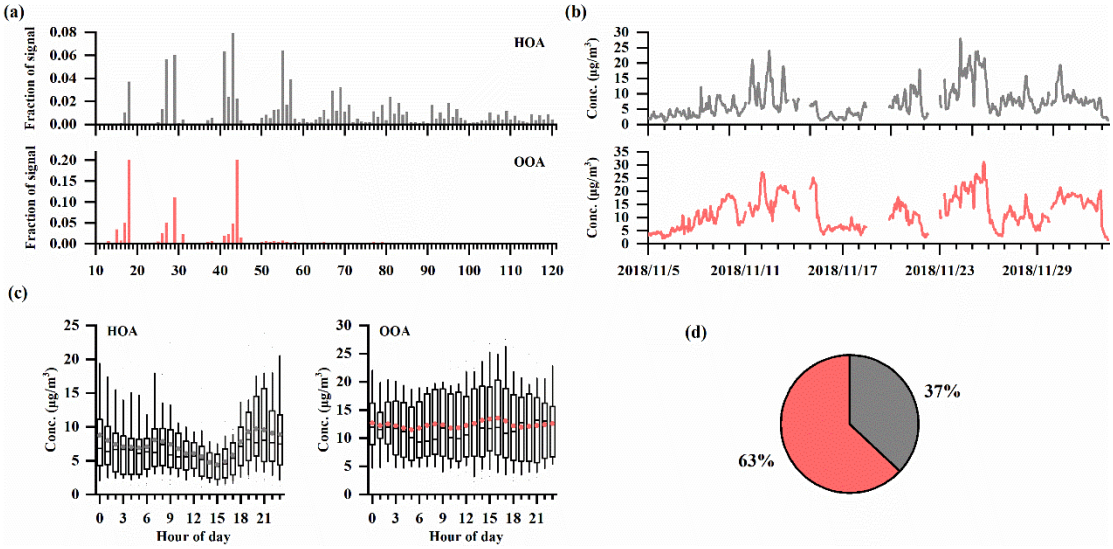

Figure S1. Summary of the mass spectra (a), time series (b), diurnal variations (c), and proportion of HOA and OOA (d) resolved from PMF model.

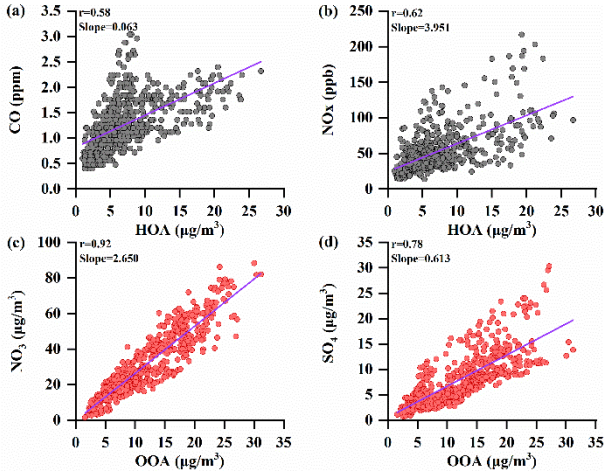

Figure S2. Scatter plots of HOA vs. CO (a), HOA vs NOx (b), OOA vs. nitrate (c), and OOA vs sulfate (d) of the measurements.

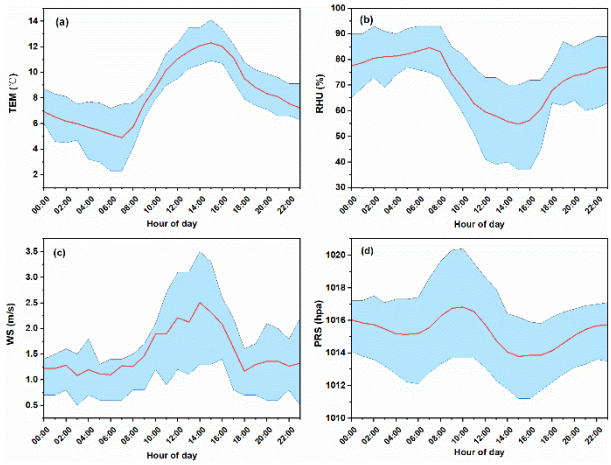

Figure S3. Diurnal variations of the meteorology parameters including temperature (a), RH (b), wind speed (c), and air pressure (d).

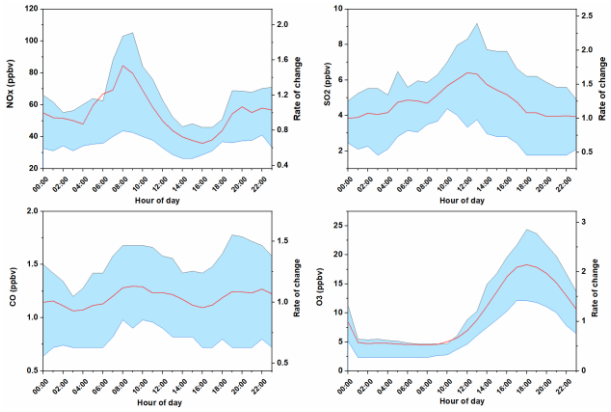

Figure S4. Diurnal variations of the inorganic gases including NO_X (a), SO_2 (b), CO (c), and O_3 (d).

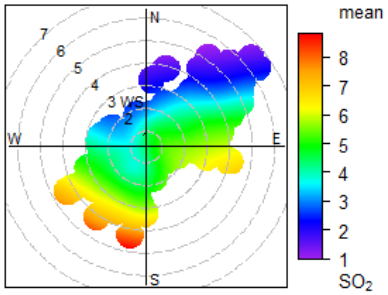

Figure S5. Concentration Variation of SO_2 with wind speed (m s^{-1}) and direction in Xinxiang.

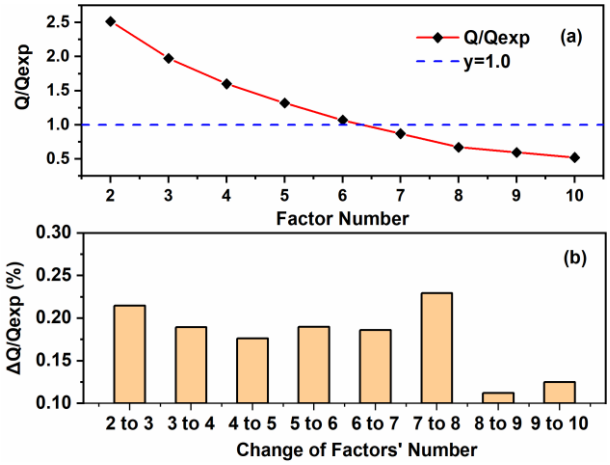

Figure S6. The value (a) and the relative change (b) of Q/Q_{exp} ratio with change in factor number.

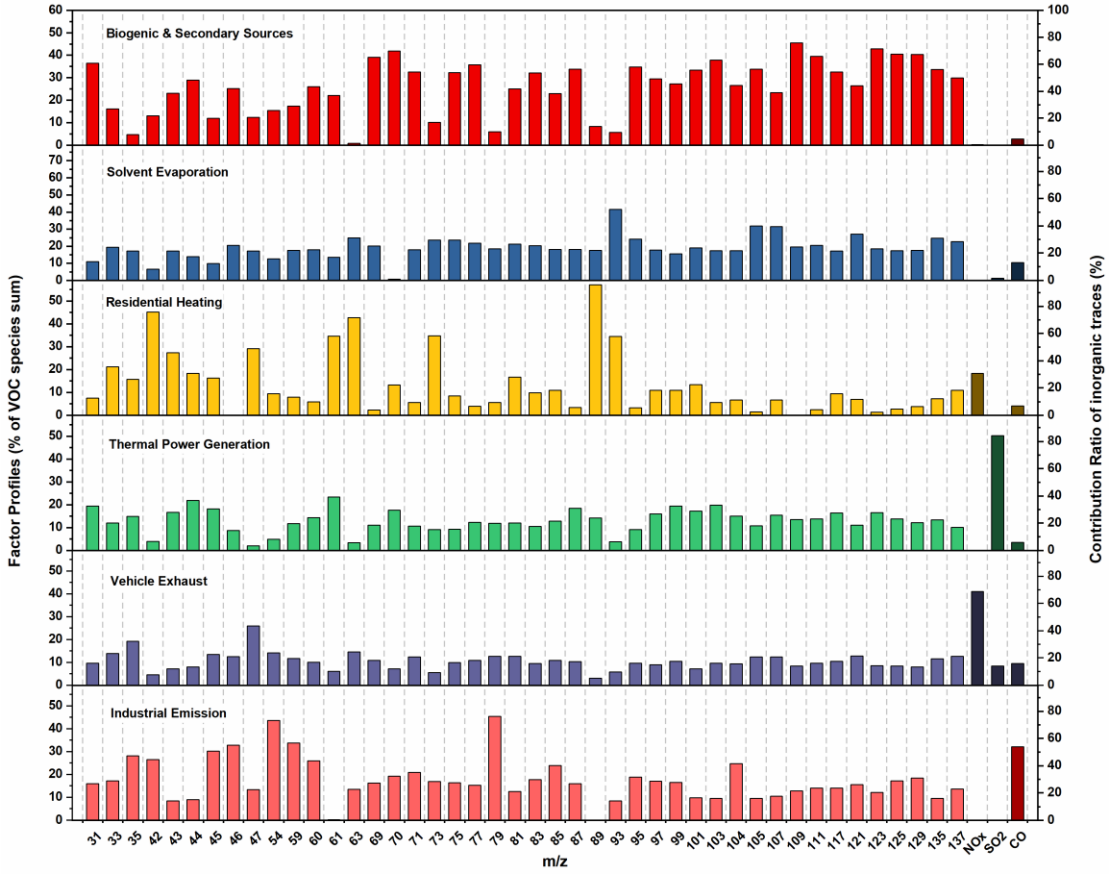

Figure S7. Factor profiles of major emission sources resolved by the positive matrix factorization (PMF) model. The bright columns represent VOC profiles corresponding to the left Y-axis, and the dark columns represent inorganic tracer profiles corresponding to the right Y-axis.

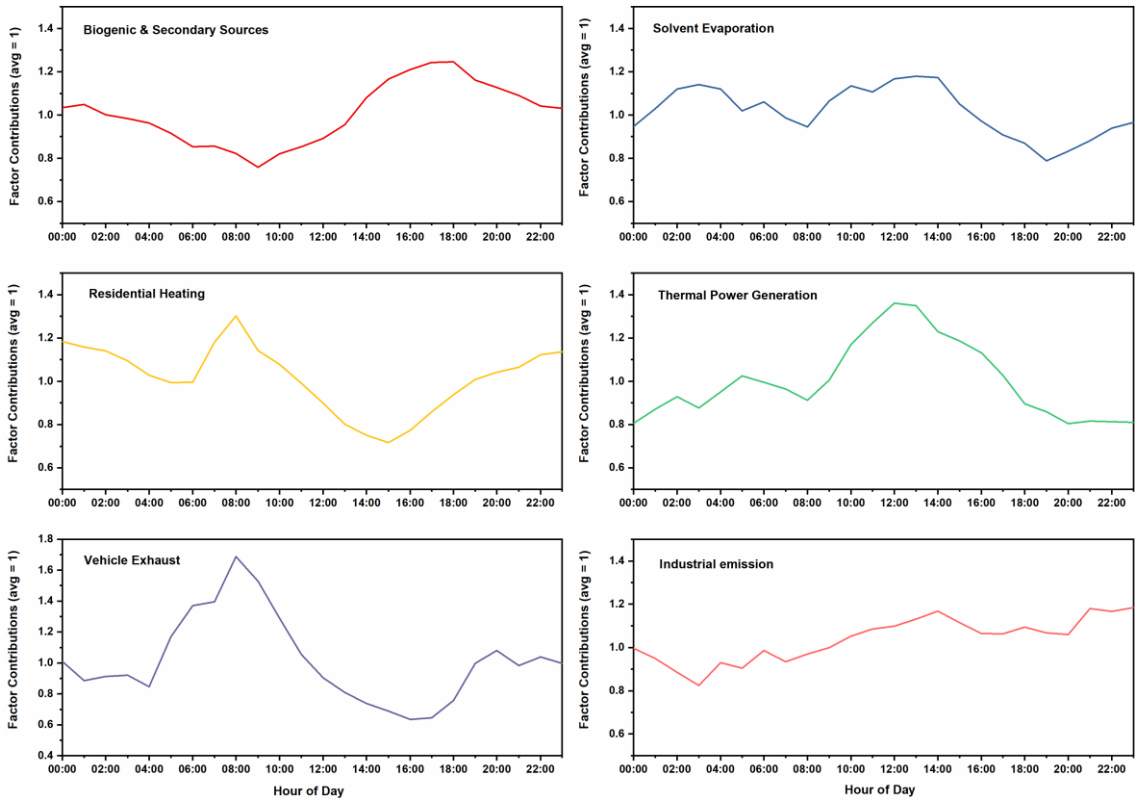

Figure S8. Diurnal variations of the source emission strength resolved by PMF model.

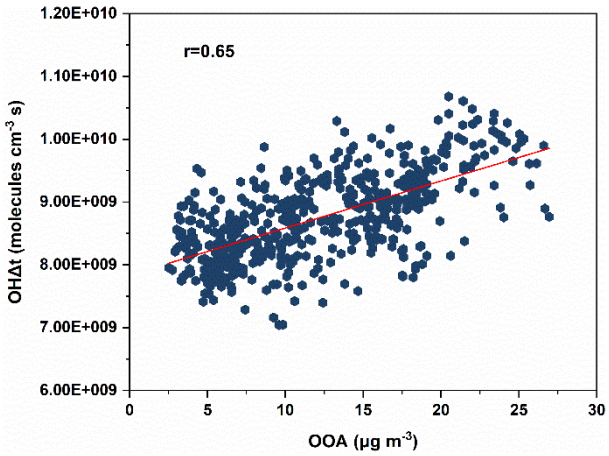

Figure S9. The correlation curve of OH exposure (OHΔt) versus OA concentration.

.

Table S1. Identified Compounds from Mass List of PTR-MS

Mass	Formula	Species	Mass	Formula	Species
31	CH_2OH^+	Formaldehyde	81	$C_6H_9^+$	Monoterpenes fragment
33	CH_4OH^+	Methanol			PAH fragment
35	H_2SH^+	H_2S	83	$C_5H_6OH^+$	Methyl furan
42	$C_2H_3NH^+$	Acetonitrile		$C_6H_{11}^+$	Methylcyclopentane
43	$C_2H_3O^+$	Fragmentation from acetic acid	85	$C_4H_4O_2H^+$	Furanone
				$C_5H_8OH^+$	Cyclopentanone
	$C_3H_7^+$	Fragmentation from hydrocarbons and propanol	87	$C_4H_6O_2H^+$	Butanedione; Methacrylic acid
44	$CHNOH^+$	Isocyanic acid		$C_5H_{10}OH^+$	MBO; Pentanones + Pentanal
45	$C_2H_4OH^+$	Acetaldehyde			
46	NO_2^+	PAN fragmentation; Methylnitrate; Other nitrogen-containing compounds	89	$C_3H_4O_3H^+$	Pyruvic acid
				$C_4H_8O_2H^+$	Butyric acid
			93	$C_7H_8H^+$	Toluene
			95	$C_6H_6OH^+$	Phenol
47	$CH_2O_2H^+$	Formic acid	97	$C_5H_4O_2H^+$	Furfural
	$C_2H_6OH^+$	Ethanol		$C_7H_{13}H^+$	Methylcyclohexane
54	$C_3H_3NH^+$	Acrylonitrile		$C_4H_2O_3H^+$	Maleic anhydride
59	$C_3H_6OH^+$	Acetone + Propanal	99	$C_5H_6O_2H^+$	Furfuryl alcohol
60	$C_2H_5NOH^+$	Acetamide		$C_6H_{10}OH^+$	Hexenals; Cyclohexanone
	$C_3H_9NH^+$	Trimethylamine			
61	$C_2H_4O_2H^+$	Acetic acid; Glycolaldehyde; Fragmentation of ethyl acetate	101	$C_6H_{12}OH^+$	Hexanal
			103	$C_5H_{10}O_2H^+$	Pentanoic acid
63	$C_2H_6SH^+$	Dimethyl sulfide	104	$C_7H_5NH^+$	Benzonitrile
69	$C_4H_4OH^+$	Furan	105	$C_8H_8H^+$	Styrene
	$C_5H_8H^+$	Isoprene and Fragmentation of MBO; Fragmentation of cyclohexenes	107	$C_7H_6OH^+$	Benzaldehyde
				$C_8H_{10}H^+$	C8 aromatics
			109	$C_7H_8OH^+$	Cresols
70	$C_4H_7NH^+$	Butane nitrile; pyrroline	111	$C_6H_6O_2H^+$	Benzenediols; Methylfurfural
71	$C_4H_6OH^+$	Methyl vinyl ketone + Methacrolein; Crotonaldehyde; ISOPOOH		$C_8H_{14}H^+$	C2 cyclohexanes
			117		OVOCs
	$C_5H_{11}^+$	Fragmentation from hydrocarbons	121	$C_9H_{12}H^+$	C9 aromatics
			123	$C_8H_{10}OH^+$	C2 phenols
73	$C_4H_8OH^+$	Methyl ethyl ketone + butanals	125	$C_7H_8O_2H^+$	Guaiacol; Methyl benzenediols
	$C_3H_4O_2H^+$	Methylglyoxal; acrylic acid	129	$C_{10}H_8H^+$	Naphthalene
75	$C_3H_6O_2H^+$	Hydroxyacetone; Propanoic acid	135	$C_{10}H_{14}H^+$	C10 aromatics
77	$C_2H_4O_3H^+$	PAN; Peracetic acid	137	$C_{10}H_{16}H^+$	Monoterpenes
79	$C_6H_6H^+$	Benzene			

Table S2. The list of beginning time of canister sampling.

Sequence Number	Time	Sequence Number	Time	Sequence Number	Time
1	2018/11/11 10:00	10	2018/11/19 12:30	19	2018/11/30 18:00
2	2018/11/11 15:30	11	2018/11/23 14:00	20	2018/12/1 9:00
3	2018/11/13 11:00	12	2018/11/24 9:30	21	2018/12/1 12:00
4	2018/11/14 11:00	13	2018/11/25 10:30	22	2018/12/4 12:00
5	2018/11/14 16:30	14	2018/11/26 13:00	23	2018/12/9 8:25
6	2018/11/15 13:00	15	2018/11/28 12:30	24	2018/12/10 8:25
7	2018/11/16 11:00	16	2018/11/29 9:30	25	2018/12/11 8:25
8	2018/11/18 13:30	17	2018/11/29 17:30	26	2018/12/13 8:21
9	2018/11/18 15:00	18	2018/11/30 9:30	27	2018/12/14 8:29

Table S3. SOA yields (%) of various VOCs under high-NOx condition.

Species	Yield	Species	Yield
Alkanes		**Others**	
Cyclopentane	4.6[a]	Phenol	26[d]
C6 Cycloalkanes	4.6[a]	Cresols	7[b]
Heptane	1[a]	Acetone	0.78[c]
Methyl-cyclohexane	14[a]	Methyl ethyl ketone	0.78[c]
Octane	4.8[a]	Valeraldehyde	9.3[c]
C8 Branched alkanes	4.8[a]	Hexanaldehyde	9.3[c]
Undecane	31[a]	Pentanol	31[d]
Dodecane	17[a]	Hexanol	31[d]
Aromatics		Nonanol	31[d]
Benzene	27[b]	Isoprene	0.79[c]
Toluene	108[b]	Terpenes	0.24[d]
Styrene	4.5[c]	Chlorobenzene	5.4[c]
Xylene	7.6[b]	1,3-Dichloro-benzene	1.6[c]
Ethylbenzene	5.4[c]	1,4-Dichloro-benzene	1.6[c]
n/iso-Propylbenzene	1.6[c]	Other halogenated hydrocarbons	3.5[c]
m/p/o-Ethyltoluene	5.6[c]		
TMB	3.2[b]		
m/p-Diethylbenzene	6.3[c]		

[a] Yields are obtained from (Lim and Ziemann, 2009).

[b] Yields are recalculated from two-product model based on (Ng et al., 2007) and (Henry et al., 2008).

[c] Yields are referred from the nationally averaged SOA yields (Wu and Xie, 2018).

[d] Yields are replaced with the fractional aerosol coefficient (FAC) value (Grosjean and Seinfeld, 1989).

[e] Yields are corrected by vapor loss biases (R_{wall}). According to (Zhang et al., 2014), the R_{wall} of toluene is around 10 in the current condition, and the R_{wall} of dodecane, benzene and xylene are 1.16, 1.25, and 1.2, respectively. The other species in [a] and [b] are corrected With a R_{wall} of 1.16, as a recent study performed (Gao et al., 2019).

References

Barletta, B., Meinardi, S., Rowland, F. S., Chan, C. Y., Wang, X. M., Zou, S. C., Chan, L. Y., and Blake, D. R.: Volatile organic compounds in 43 Chinese cities, Atmos. Environ., 39, 5979-5990, 10.1016/j.atmosenv.2005.06.029, 2005.

Coeur Tourneur, C., Henry, F., Janquin, M. A., and Brutier, L.: Gas-phase reaction of hydroxyl radicals with m-, o- and p-cresol, Int. J Chem. Kinet., 38, 553-562, 10.1002/kin.20186, 2006.

Gao, Y., Wang, H., Zhang, X., Jing, S. a., Peng, Y., Qiao, L., Zhou, M., Huang, D. D., Wang, Q., Li, X., Li, L., Feng, J., Ma, Y., and Li, Y.: Estimating Secondary Organic Aerosol Production from Toluene Photochemistry in a Megacity of China, Environ. Sci. Technol. 53, 8664-8671, 10.1021/acs.est.9b00651, 2019.

Ge, B., Wang, Z., Lin, W., Xu, X., Li, J., Ji, D., and Ma, Z.: Air pollution over the North China Plain and its implication of regional transport: A new sight from the observed evidences, Environ. Pollut., 234, 29-38, 10.1016/j.envpol.2017.10.084, 2018.

Grosjean, D., and Seinfeld, J. H.: Parameterization of the formation potential of secondary organic aerosols, Atmos. Environ., 23, 1733-1747, 10.1016/0004-6981(89)90058-9, 1989.

Henry, F., Coeur-Tourneur, C., Ledoux, F., Tomas, A., and Menu, D.: Secondary organic aerosol formation from the gas phase reaction of hydroxyl radicals with m-, o- and p-cresol, Atmos. Environ., 42, 3035-3045, https://doi.org/10.1016/j.atmosenv.2007.12.043, 2008.

Li, B., Ho, S. S. H., Gong, S., Ni, J., Li, H., Han, L., Yang, Y., Qi, Y., and Zhao, D.: Characterization of VOCs and their related atmospheric processes in a central Chinese city during severe ozone pollution periods, Atmos. Chem. Phys., 19, 617-638, 10.5194/acp-19-617-2019, 2019.

Lim, Y. B., and Ziemann, P. J.: Effects of Molecular Structure on Aerosol Yields from OH Radical-Initiated Reactions of Linear, Branched, and Cyclic Alkanes in the Presence of NOx, Environ. Sci. Technol. 43, 2328-2334, 10.1021/es803389s, 2009.

Mallik, C., Mahapatra, P. S., Kumar, P., Panda, S., Boopathy, R., Das, T., and Lal, S.: Influence of regional emissions on SO_2 concentrations over Bhubaneswar, a capital city in eastern India downwind of the Indian SO_2 hotspots, Atmos. Environ., 209, 220-232, 10.1016/j.atmosenv.2019.04.006, 2019.

Ng, N. L., Kroll, J. H., Chan, A. W. H., Chhabra, P. S., Flagan, R. C., and Seinfeld, J. H.: Secondary organic aerosol formation from m-xylene, toluene, and benzene, Atmos. Chem. Phys., 7, 3909-3922, 10.5194/acp-7-3909-2007, 2007.

Roberts, J. M., Veres, P. R., VandenBoer, T. C., Warneke, C., Graus, M., Williams, E. J., Lefer, B., Brock, C. A., Bahreini, R., Öztürk, F., Middlebrook, A. M., Wagner, N. L., Dubé, W. P., and de Gouw, J. A.: New insights into atmospheric sources and sinks of isocyanic acid, HNCO, from recent urban and regional observations, J Geophys. Res.-Atmos.,119, 1060-1072, 10.1002/2013jd019931, 2014.

Sarkar, C., Sinha, V., Sinha, B., Panday, A. K., Rupakheti, M., and Lawrence, M. G.: Source apportionment of NMVOCs in the Kathmandu Valley during the SusKat-ABC international field campaign using positive matrix factorization, Atmos. Chem. Phys., 17, 8129-8156, 10.5194/acp-17-8129-2017, 2017.

Taipale, R., Ruuskanen, T. M., Rinne, J., Kajos, M. K., Hakola, H., Pohja, T., and Kulmala, M.: Technical Note: Quantitative long-term measurements of VOC concentrations by PTR-MS - measurement, calibration, and volume mixing ratio calculation methods, Atmos. Chem. Phys., 8, 6681-6698, 10.5194/acp-8-6681-2008, 2008.

Wu, R., and Xie, S.: Spatial Distribution of Secondary Organic Aerosol Formation Potential in China Derived from Speciated Anthropogenic Volatile Organic Compound Emissions, Environ. Sci. Technol. 52, 8146-8156, 10.1021/acs.est.8b01269, 2018.

Yan, Y., Yang, C., Peng, L., Li, R., and Bai, H.: Emission characteristics of volatile organic compounds from coal-, coal gangue-, and biomass-fired power plants in China, Atmos. Environ., 143, 261-269, https://doi.org/10.1016/j.atmosenv.2016.08.052, 2016.

Yang, W., Zhang, Y., Wang, X., Li, S., Zhu, M., Yu, Q., Li, G., Huang, Z., Zhang, H., Wu, Z., Song, W., Tan, J., and Shao, M.: Volatile organic compounds at a rural site in Beijing: influence of temporary emission control and wintertime heating, Atmos. Chem. Phys., 18, 12663-12682, 10.5194/acp-18-12663-2018, 2018.

Yuan, B., Shao, M., Lu, S., and Wang, B.: Source profiles of volatile organic compounds associated with solvent use in Beijing, China, Atmos. Environ., 44, 1919-1926, https://doi.org/10.1016/j.atmosenv.2010.02.014, 2010.

Zhang, B., Zhao, B., Zuo, P., Huang, Z., and Zhang, J.: Ambient peroxyacyl nitrate concentration and regional transportation in Beijing, Atmos. Environ., 166, 543-550, https://doi.org/10.1016/j.atmosenv.2017.07.053, 2017.

Zhang, X., Cappa, C. D., Jathar, S. H., McVay, R. C., Ensberg, J. J., Kleeman, M. J., and Seinfeld, J. H.: Influence of vapor wall loss in laboratory chambers on yields of secondary organic aerosol, P Natl. Acad. Sci. US., 111, 5802-5807, 10.1073/pnas.1404727111, 2014.

Zheng, H., Kong, S., Xing, X., Mao, Y., Hu, T., Ding, Y., Li, G., Liu, D., Li, S., and Qi, S.: Monitoring of volatile organic compounds (VOCs) from an oil and gas station in northwest China for 1 year, Atmos. Chem. Phys., 18, 4567-4595, 10.5194/acp-18-4567-2018, 2018.

Zhou, X., Li, Z., Zhang, T., Wang, F., Wang, F., Tao, Y., Zhang, X., Wang, F., and Huang, J.: Volatile organic compounds in a typical petrochemical industrialized valley city of northwest China based on high-resolution PTR-MS measurements: Characterization, sources and chemical effects, Sci. Total Environ., 671, 883-896, https://doi.org/10.1016/j.scitotenv.2019.03.283, 2019.